

Mott-Enhanced Exciton Condensation in a Hubbard bilayer

Samuele Giuli,^{1,*} Adriano Amaricci,² and Massimo Capone^{1,2}

¹*International School for Advanced Studies (SISSA), via Bonomea 265, 34136 Trieste, Italy*

²*CNR-IOM, via Bonomea 265, 34136 Trieste, Italy*

(Dated: July 17, 2023)

We study the conditions to realize an excitonic condensed phase in an electron-hole bilayer system with local Hubbard-like interactions at half-filling, where we can address the interplay with Mott localization. Using Dynamical Mean-Field Theory, we find that an excitonic state is stable in a sizeable region of a phase diagram spanned by the intra-layer (U) and inter-layer (V) interactions. The latter term is expected to favour the excitonic phase which is indeed found in a slice of the phase diagram with $V > U$. Remarkably, we find that when U is large enough, the excitonic region extends also for $U > V$ in contrast with naive expectations. The extended stability of the excitonic phase can be linked to in-layer Mott localization and inter-layer spin correlations. Using a mapping to a model with attractive inter-layer coupling, we fully characterize the condensate phase in terms of its superconducting counterpart, thereby addressing its coherence and correlation length.

I. INTRODUCTION

The condensation of excitons in a macroscopic quantum state has been proposed soon after the success of BCS theory of superconductivity^{1,2} owing to the similarities between the Cooper pairs created by the binding of two electrons, and the excitons, bound states formed by an electron and a hole. However, the observation of excitonic phases has long eluded the experimental effort, mainly because of the short lifetimes of the excitons due to electron-hole recombination processes.

The developments in the engineering of devices and heterostructures have provided ideal platforms to observe exciton condensation (EC), which has been indeed proposed and reported in quantum-Hall bilayers^{3,4}, graphene double bilayers⁵⁻⁸ and semiconductors quantum wells^{9,10}. Excitonic ordering has also been recently reported also in bulk solids¹¹⁻¹⁸

Bilayer structures are arguably ideal platforms to observe condensation of spatially indirect excitons composed by holes and electrons belonging to different layers, for which recombination is essentially inhibited by the presence of a dielectric material between the layers. Quantum Monte Carlo calculations for electron-hole gases coupled by the long-range Coulomb interaction¹⁹⁻²¹ have indeed shown that an excitonic phase is stable at very low densities, a result which has been confirmed by simulations of double bilayer graphene^{5,6}.

In an analogous lattice model with local interactions some indication of exciton condensation has been found away from half-filling²² and in the half-filled system when the interlayer interaction is larger than the intra-layer repulsion^{23,24}. Similar models have been investigated using Dynamical Mean-Field Theory (DMFT). In Ref. 25 the competition between EC and s-wave superconductivity has been addressed in a model without intra-layer repulsion. A variety of two-orbital models including, e.g., energy splitting between bands, the Hund's coupling and including non-trivial topology have also been found to host excitonic states in some regions of parameters²⁶⁻³¹.

In this work we aim at identifying a generic mechanism connecting strong correlation physics and excitonic phases which can be used to gain a deeper insight on results on more involved and richer models for specific systems. In particular, we address the interplay between the EC and Mott physics, the most direct fingerprint of correlations, in an idealized model for an electron-hole bilayer system with local Hubbard-like interactions. Our focus is on the relative role of the intra-layer (U) and inter-layer (V) interactions. We consider the system at half-filling, where a Mott transition can take place, so that our phase diagram will be characterized by the competition/interplay between Mott insulating and EC phases.

The paper is organized as follows: In Sec. II we introduce the model, our implementation of Dynamical Mean-Field Theory and the relevant observables we consider. In Sec. III we present the normal-phase results where we discard excitonic ordering, while Sec. IV is devoted to the results for the EC phase. Sec. V reports our concluding remarks.

II. MODEL AND METHOD

We consider a two-layer Hubbard model with a local interaction term:

$$H = - \sum_{\langle ij \rangle \sigma m} t_m c_{i\sigma m}^\dagger c_{j\sigma m} + H.c. - \mu \sum_{i\sigma m} n_{i\sigma m} + U \sum_{im} n'_{i\uparrow m} n'_{i\downarrow m} + V \sum_{i\sigma\sigma'} n'_{i\sigma A} n'_{i\sigma' B} \quad (1)$$

where $c_{i\sigma m}$ ($c_{i\sigma m}^\dagger$) is the annihilation (creation) operator of an electron on site i , layer $m = A, B$ and with spin σ , $n_{i\sigma m}$ is the number operator and $n'_{i\sigma m} = n_{i\sigma m} - 1/2$ is introduced to write the model in a particle-hole symmetric form which implies that both bands are half-filled for $\mu = 0$. We set $t_A = t$ and $t_B = \alpha t_A$. In our calculations we will consider $\alpha = -1$ in order to describe an electron-like band (A) and a hole-like band (B). U and V are both positive and they measure the intra-layer and inter-layer local screened Coulomb repulsion.

We will study an excitonic state characterized by a uniform ($q = 0$) spin-singlet excitonic order parameter (EOP)

$$\Delta_0 = \frac{1}{N} \sum_{i\sigma} \langle c_{iA\sigma}^\dagger c_{iB\sigma} \rangle \quad (2)$$

which is expected to be degenerate with spin-triplet counterparts due to the $SU(2) \times SU(2)$ spin symmetry of our model. Models including other interaction terms and material-specific features, may favour one or the other spin symmetries^{28,29,31}.

We solve the model at zero temperature using DMFT³², a state-of-the-art method which treats different interactions non perturbatively and it is particularly well suited to study the Mott transition³², strongly correlated metallic phases as well as superconductivity and other broken-symmetry states. Within DMFT the lattice model is mapped onto an impurity model which has to be solved self-consistently requiring that the impurity Green's function coincides with the local component of the lattice Green's function. We solve the impurity model at $T = 0$ using Lanczos/Arnoldi exact diagonalization (ED)³³⁻³⁵. As customary in the DMFT community, we consider a Bethe lattice with a semicircular density of states $N_m(\epsilon) = \frac{2}{\pi D_m^2} \sqrt{D_m^2 - \epsilon^2}$, where $D_m \propto t_m$ is the half-bandwidth.

In order to study the EC phase, the bath of the impurity model has to include an excitonic amplitude, analogously to the superconducting case. Using a spinorial representation where $\Psi_{k,\sigma}^\dagger = (c_{k\sigma A}^\dagger, c_{k\sigma B}^\dagger)$, where $k = 0$ identify the impurity and $k = 1, \dots, N_{bath}$ the bath levels, we can write it as

$$H_{imp}^{(0)} = \sum_{k\sigma} \begin{pmatrix} \Psi_{k\sigma}^\dagger & \Psi_{0\sigma}^\dagger \end{pmatrix} \begin{pmatrix} \mathcal{H}_{k\sigma} & V_k \cdot \mathbb{I}_2 \\ V_k \cdot \mathbb{I}_2 & 0 \end{pmatrix} \begin{pmatrix} \Psi_{k\sigma} \\ \Psi_{0\sigma} \end{pmatrix} \quad (3)$$

where \mathbb{I}_2 is the 2×2 identity and

$$\mathcal{H}_{k\sigma} = \begin{pmatrix} \epsilon_k + M_k & P_k \\ P_k & \epsilon_k - M_k \end{pmatrix} \quad (4)$$

where P_k is the inter-orbital excitonic hybridization term in the bath Hamiltonian, $\epsilon_k + (-)M_k$ is the bath energy on orbital A (B) and V_k is the hybridization between the impurity and bath site k . Within ED-DMFT we have to limit the number of bath sites to be able to solve the impurity model. We fixed the number of bath sites to be $N_{bath} = 4$ and we fixed the system at global half-filling ($\sum_{\sigma m} n_{\sigma m} = 2$) by imposing $\mu = 0$, then since we are focusing on orbitals with opposite dispersion relation we also fixed $\epsilon_k = 0 \ \forall k$ and since we focus on state with orbital half-filling, this required that for each M_k parameter on bath site k there must be another bath site k' with opposite energy $M_{k'} = -M_k$.

III. NORMAL STATE

We start our investigation from the normal state where we inhibit excitonic ordering, as well as any other broken-symmetry state like antiferromagnetism or staggered orbital ordering. This is a standard strategy which has helped to understand the Mott transition disentangling Mott localization from magnetic ordering³². For our model, a normal-state phase diagram has been reported in Ref.³⁶, but we find it useful to present our results in order to emphasize the aspects which are useful to better address the excitonic phase.

The model is expected to feature two different Mott-insulating solutions that we can easily understand from the atomic ($t_m = 0$) limit. Among all configurations with two electrons per site, the four with one electron in each layer $|\uparrow, \downarrow\rangle, |\downarrow, \uparrow\rangle, |\uparrow, \uparrow\rangle$ and $|\downarrow, \downarrow\rangle$ have energy $E_{11} = -\frac{1}{2}U$, while the two configurations with two electrons in the same layer $|\uparrow\downarrow, 0\rangle$ and $|0, \uparrow\downarrow\rangle$ have energy $E_{20} = \frac{1}{2}U - V$. Therefore the former set of states is favoured for $U > V$ and the latter for $U < V$. Hence when U and V are much larger than the hopping and $U > V$ we expect an insulator with one electron on every site of each layer. This state, that we label as U-Mott (U-MI) is expected to be unstable towards antiferromagnetic ordering if we allow for symmetry breaking. On the other hand, for $V > U$ we have an insulator where every site is in a mixture between the two solutions with one doubly occupied layer. This state, henceforth V-Mott (V-MI), would be naturally unstable towards a staggered orbital (layer) ordering.

In order to monitor the Mott localization we compute the quasiparticle weight Z_m which measures the metallicity of the system³². The progressive destruction of the metallic state is described by a reduction of Z_m from 1 (non-interacting limit) to 0 (correlated insulator). The connected local density-density correlations $C_{m,m'} = \langle n_m n_{m'} \rangle - \langle n_m \rangle \langle n_{m'} \rangle$ can be used to study the competition between the two **interaction** terms and the approach to the atomic limit insulators. The orbital symmetry implies $C_{AA} = C_{BB}$ and $C_{AB} = C_{BA}$. It is easy to see from the above discussion that the atomic $U - MI$ has $C_{AA} = 0$ and $C_{AB} = 0$, while the atomic $V - MI$ has $C_{AA} = 1$ and $C_{AB} = -1$.

In Fig. 1 we show as dotted lines the evolution of $Z_A = Z_B$ and of the inter- and intra-layer correlations C_{AA} and C_{AB} as functions of V/D for different values of U/D . The boundaries of the U-MI and V-MI phases are marked by dotted lines with crosses in the phase diagram of Fig. 2

The cuts for $U/D = 1$ and 2 in Fig. 1 clearly show a metal-insulator transition towards the V-MI state with $Z_A = 0$, $C_{AA} = 1$ and $C_{AB} = -1$. For $U/D = 3$, we find a U-MI for small V followed by a metallic region and the V-MI as V increases. For large $U/D = 4$ we have only a tiny slice of V with a metallic solution sandwiched by the two insulators.

The main feature of the normal-state phase diagram,

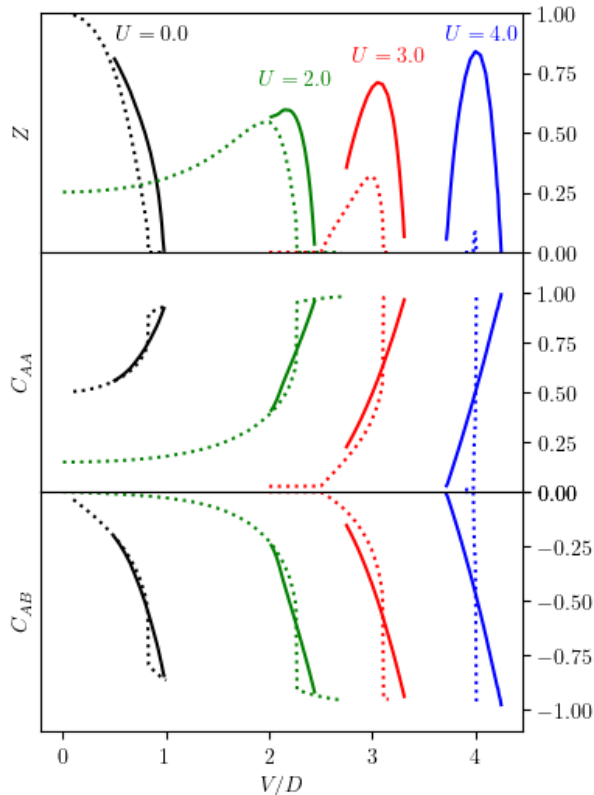


FIG. 1. Quasiparticle weight (top), intra-orbital density-density correlation (center) and inter-orbital density-density correlation (bottom), as a function of V/D for $U/D = 0.0$ (black), 2.0 (green), 3.0 (red) and 4.0 (blue). Dotted lines are data in the normal state, solid lines mark the same quantities in the excitonic phase

as already pointed out in Ref. 36, is the existence of a metallic region when U and V are comparable, even when they are so large to independently drive a Mott transition (in the absence one of the other). The region shrinks as we increase U and V but it does not close. In particular, for $U = V$ we always find a metallic solution, similarly to other models where the competition between different atomic states leads to intermediate phases which can have either a metallic^{37,38} or an insulating³⁹ nature.

IV. EXCITONIC PHASE

We now turn to solutions where the exciton condensation is allowed. The values of Z_A , C_{AA} and C_{AB} are shown as solid lines in Fig. 1 and compared with their normal-state counterparts. Indeed, the excitonic state is stable in a wide region of parameters and its onset makes the evolution from the U-MI to the V-MI smoother, thereby increasing also the quasiparticle weight.

Reporting this information on the phase diagram of Fig. 2, where the boundaries of the excitonic region are black solid lines, we clearly see that the EC region is

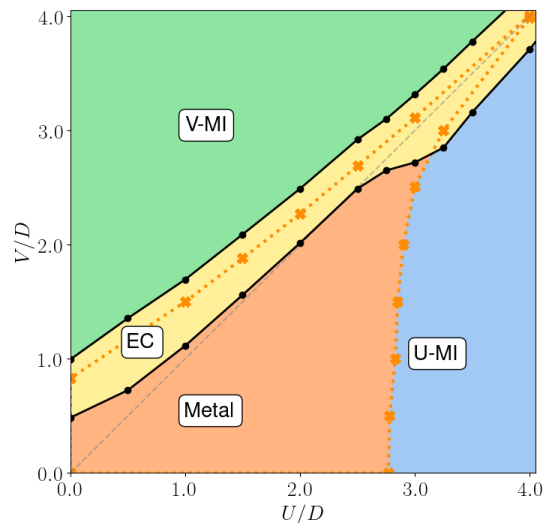


FIG. 2. V vs U Ground State Phase Diagram. In *yellow* the region of EC phase, in *orange* the metallic phase, in *blue* the U-Mott insulator and in *green* the V-Mott one. The dashed lines with crosses symbols indicate the two Mott-transition boundaries in the normal state, while the gray dashed line highlight the $U = V$ line.

roughly centered around the normal state transition towards the V-Mott state. The picture is simple: Increasing V , before the interaction is large enough to drive the system insulating, it leads to the binding of **electrons and holes on different layers into excitons**. However, the effect of U changes the position and the nature of the transition.

For small and moderate U the EC establishes only when V prevails over U (above the $V = U$ line, marked with a dashed grey line) in agreement with previous work²³⁻²⁵.

A much less expected result emerges when we increase U and we approach the boundary of the U-MI phase. Here we find that the stability region of the EC increases and, remarkably, it extends in the region where $U < V$ signaling a non-trivial intrinsic many-body effect due to the interplay of the two interactions. As a result, for $U \gtrsim 3D$, the whole metallic region between the two Mott insulators is replaced by an excitonic state.

The positive effect of the Hubbard repulsion on the excitonic order is evident in Fig. 3 (a), where we plot the order parameter Δ as a function of V for the same cuts of Fig. 1. Here we show that the EC for large U is not only stable in a wider range of V , but its amplitude is also larger. For instance, for $U/D = 4$ the maximum value of Δ is more than twice the $U = 0$ maximum. For every value of U , the transition from the metal to the EC appears of first-order, while the transition from the EC to the V-MI state is associated with a continuously vanishing Δ .

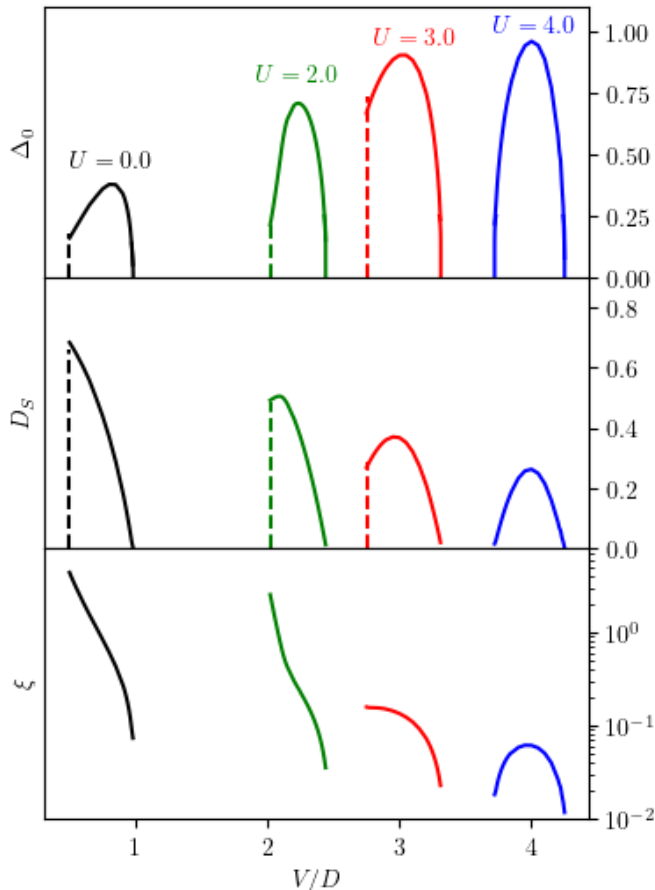


FIG. 3. Excitonic order parameter Δ_0 (top), stiffness D_s (center) and coherence length ξ for (from left to right) $U/D = 0.0, 2.0, 3.0, 4.0$ with the same color codes of Fig. 1. The vertical dashed line indicate the first order Metal-EC phase transition.

A. Exciton Ordering and Mott physics

In this section we link the enhancement of the EC region for $V < U$ and large U/D to the magnetic correlation between orbitals near the V-MI phase that is enhanced by the nearby U-MI phase. The main effect of U is to drive a standard Mott localization within each layer. Hence the double occupation on each layer d_m is strongly reduced. For a half-filled non-magnetic system this reflects directly in the formation of local moments as measured by $\langle S_m^z S_m^z \rangle = \frac{1}{4} \langle (n_{m,\uparrow} - n_{m,\downarrow})^2 \rangle = \frac{1}{2} (\frac{1}{2} - d_m)$ which approaches $1/4$. While the spins on the two layers are uncorrelated in the normal state, when we reach the EC region and $U \gtrsim 3D$ the inter-layer spin correlations $\langle S_A^z S_B^z \rangle$ become sizeable and negative eventually approaching the limit $-1/4$.

The local quantum state (computed from the impurity model within DMFT) approaches for large U $|\psi\rangle \sim \frac{1}{\sqrt{2}}(|\uparrow_A \downarrow_B\rangle + |\uparrow_B \downarrow_A\rangle)$ for which $\langle S_A^z S_A^z \rangle = \frac{1}{4}$ and $\langle S_A^z S_B^z \rangle = -\frac{1}{4}$.

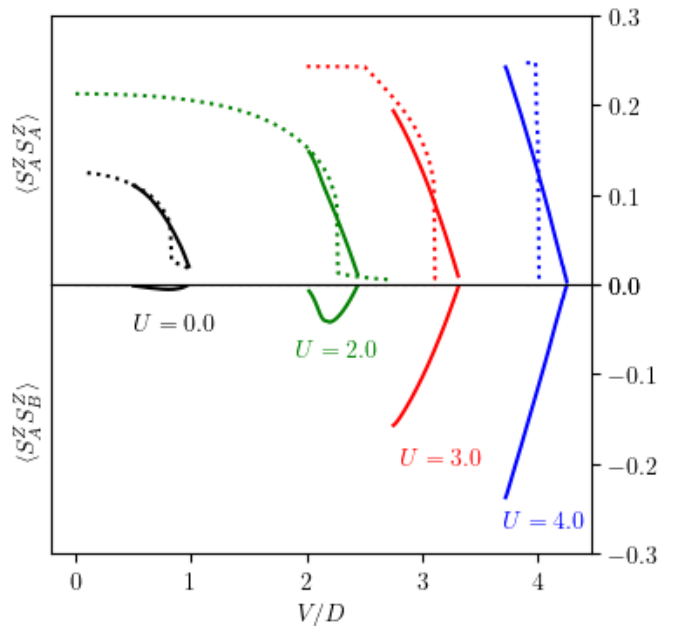


FIG. 4. Local magnetic moments (intra-orbital spin correlations) (top) and inter-orbital magnetic correlation (bottom). Dotted and solid lines indicate, respectively, the normal and the excitonic phase solution. Data are for $U/D = 0.0$ (black), 2.0 (green), 3.0 (red) and 4.0 (blue).

Note however that the interplay between Mott localization and exciton ordering is not trivial. The singlet atomic excitonic state is indeed a linear combination of $|\uparrow_A \downarrow_B\rangle$ and $|\uparrow_B \downarrow_A\rangle$ which are favoured by increasing U , but also of the states $|\uparrow_A \downarrow_A, 0\rangle$ and $|0, \uparrow_B \downarrow_B\rangle$, which are instead depleted by U . Hence, while the magnetic correlations develop approaching the U-Mott state, they first contribute to the onset of excitonic ordering, but as we exceed a given "optimal" distance from the Mott state, the EOP decreases, leading to the existence of a bell-shaped behavior of the order parameter.

We finally notice that the spin-singlet correlations follow from our choice to study spin-singlet excitons, and we expect the same picture to hold for spin-triplet exciton. The key idea is that Mott localization within each layer leads to localized moments which are naturally prone to acquire any inter-layer correlation when exciton ordering is allowed. Finally, in the U-MI state the EOP vanishes and the $SU(2) \times SU(2)$ spin symmetry with four independent ground states is recovered.

B. Characterizing the Excitonic State via a mapping on Superconductivity

A particle-hole transformation on layer B:

$$c_{i\sigma B}^\dagger \rightarrow c_{i\sigma B}(-1)^\sigma \quad (5)$$

maps our model for $\alpha = -1$ onto a two-orbital model with the same form of Eq. (1) in which the two orbitals share the same hopping $t_A = t_B = t$ and the inter-orbital interaction becomes attractive ($-V$), while the intra-layer remains repulsive. This model can indeed host an inter-orbital s-wave superconducting state, which maps on our excitonic state via the same particle-hole transformation (5). We can exploit this mapping to compute some observable which characterize the superconducting state and allow to better characterize the EC.

The superfluid stiffness D_s ⁴⁰ is a crucial parameter that controls the critical temperature. It measures the coherence of the superconducting state and its rigidity to fluctuations of the phase of the order parameter. Indeed, a superconductor with small D_s has a small critical temperature even if the zero-temperature modulus of the order parameter is large, as it happens in the strong-coupling limit in a single-orbital attractive Hubbard model⁴¹ In the effective model with inter-layer attraction $-|V|$ obtained via the transformation (5) D_s reads

$$\frac{D_S}{\pi e^2} = \langle -E_{kin} \rangle - \chi_{jj}(\mathbf{q} \rightarrow 0, \omega = 0) \quad (6)$$

where j is the current operator and E_{kin} is the expectation value of the hopping part of the Hamiltonian. For a Bethe lattice we obtain⁴¹

$$\frac{D_S^{ex}}{e^2 \pi} = -\frac{4\alpha}{\beta} \sum_{i\omega_n, \sigma} \int d\varepsilon V(\varepsilon) D(\varepsilon) |G_{AB}(\varepsilon, i\omega_n)|^2 \quad (7)$$

where $V(\varepsilon) = \frac{4t^2 - \varepsilon^2}{2}$ is the square of the current vertex for orbital A and $\alpha = t_B/t_A$ (See Appendix A for derivation).

We underline that the total current of the attractive model corresponds, in model (1), to the operator

$$j_{ex}(\mathbf{q}, i\omega_n) = j_A(\mathbf{q}, i\omega_n) - j_B(\mathbf{q}, i\omega_n), \quad (8)$$

which is clearly different from the current operator associated with the total charge. Hence, the D_s can be considered a real superfluid stiffness only for the auxiliary attractive model.

Yet, D_s provides direct also information about the coherence and stability properties, which translates into an analogous information about the EC phase of our model (1).

The coherence length ξ has indeed naturally the same meaning in the two frameworks, namely it measures the length over which the constituents of the pair/exciton retain quantum coherence. It is given by^{42,43}

$$\xi^2 = \frac{\sum_{\mathbf{k}} |\nabla_{\mathbf{k}} F(\mathbf{k})|^2}{\sum_{\mathbf{k}} |F(\mathbf{k})|^2} \quad (9)$$

where

$$F(\mathbf{k}) = \sum_{i\omega_n} e^{i\omega_n 0^+} G_{AB}(\varepsilon_{\mathbf{k}}, i\omega_n) \quad (10)$$

The results for D_s and ξ are reported in panels (b) and (c) of Fig. 3 in order to compare their behavior with the EOP. The results for $U = 0$ are qualitatively similar to an attractive model and they reflect the BCS to Bose-Einstein Condensate (BEC) crossover as a function of the coupling. Indeed both D_s and ξ are maximal in the weak-coupling side and they decrease as the interaction grows.

Increasing $|V|$ we have a progressive reduction of the coherence length, associated with more localized pairs/excitons characteristic of the BEC limit. Also D_s decreases as result of the smaller coherence of the pairs/excitons and it actually vanishes at the continuous transition to the V-MI state.

When we introduce and increase U , we find an important difference on the "weak-coupling" side of the crossover. Indeed both D_s and ξ are depleted also close to the smallest values of V required to establish the EC. As a result, for large U the two quantities have a maximum around the $U \sim V$ line. These results clearly confirm the U -induced localization of the excitons that we discussed above and the crucial role of the interplay between the two interactions to induce an EC for $V < U$.

V. CONCLUSIONS

We used DMFT to assess the existence of an excitonic state in the zero-temperature phase diagram of a two-layer Hubbard model with intra-layer (U) and inter-layer (V) density-density repulsive interactions. Working at half filling, we can study how the excitonic long-range order is affected by the Mott physics.

We find a sizeable region of exciton ordering when the two interactions are comparable. The transition from EC phase to the Mott insulating phase is continuous, while the transition from Metal to EC is of the first order.

For small and intermediate U , the excitonic state is present only if $V > U$. On the other hand, for $U \gtrsim 3D$ i.e., close to a standard Mott transition within each layer, we find an exciton state also when $V < U$, signaling a non-trivial interplay in which quantum fluctuations play an active role.

We have indeed shown that the enlargement of the excitonic phase in the proximity of the intra-layer Mott transition can be connected with the U -driven development of local magnetic moments that, in turn, favour magnetic correlations between the two layers (singlets in our case). We expect this mechanism to be general, and in particular, to be present also for models where the exciton and the magnetic correlations have a triplet symmetry.

Exploiting a simple mapping onto a model with attractive inter-layer interactions, we have been able to further characterize the excitonic state. The coherence length, which has essentially the same interpretation of that of a superconductor, shows that the proximity to the V -driven Mott state leads to localized pairs with very

short coherence length. Analogously, the equivalent of the superconducting superfluid stiffness shows that the coherence of the EC state tends to vanish when the V-Mott insulator is reached. In other words, when we approach the Mott transition, the EC state is driven towards the strong-coupling limit, which in the superconducting language corresponds to the BEC limit⁴¹. We notice in passing that the BEC nature and its evolution from a BCS limit can be experimentally assessed via both thermodynamic⁴¹ and spectral properties^{44,45}. These results further strengthen our picture where the charge localization induced by U is central in the stabilization of the excitonic condensate for $V < U$ and in determining its properties.

The existence of excitonic states for $V < U$ is important because in a real bilayer system, or in a multi-orbital correlated material, we always expect $V < U$. We notice however that an electron-phonon coupling of the Holstein type (coupled with the total local electron density) can effectively reduce U , making in principle the effective U closer or even smaller than V ^{39,46,47}.

As we anticipated in the introduction, our model has been introduced as the minimal model for a bilayer sys-

tem in which excitonic phases can be present and, at the same time, Mott physics is effective. The results we have obtained have to be considered as a basis to build the understanding of richer and more involved models including, among others, different and more complex hopping structures, energy difference and/or hybridization between the two bands and a richer structure of the interactions.

ACKNOWLEDGEMENTS

We acknowledge funding by MUR through the PRIN 2017 (Prot. 20172H2SC4 005), PRIN 2020 (Prot. 2020JLZ52N 002) programs, National Recovery and Resilience Plan (NRRP) MUR Project No. PE0000023-NQSTI and ICSC-Centro Nazionale di Ricerca in High Performance Computing, Big Data and Quantum Computing, funded by European Union – NextGenerationEU (Grant number CN00000013) - Mission 4 Component 2 Investments 1.3 and 1.4.

* Correspondence email address: sgiuli@sissa.it

¹ L. V. Keldysh and A. N. Kozlov, *Sov. Phys. JETP* **27**, 521 (1967).

² Y. Lozovik and V. Yudson, *Sov. Phys. JETP* **44**, 389 (1976).

³ I. B. Spielman, J. P. Eisenstein, L. N. Pfeiffer, and K. W. West, *Phys. Rev. Lett.* **87** (2001), 10.1103/PhysRevLett.87.036803.

⁴ J. P. Eisenstein and A. H. MacDonald, *Nature* **432**, 691 (2004).

⁵ G. W. Burg, N. Prasad, K. Kim, T. Taniguchi, K. Watanabe, A. H. MacDonald, L. F. Register, and E. Tutuc, *Phys. Rev. Lett.* **120** (2018), 10.1103/PhysRevLett.120.177702.

⁶ J. Li, T. Taniguchi, K. Watanabe, J. Hone, and C. Dean, *Nat. Phys.* **13**, 751 (2017).

⁷ A. Perali, D. Neilson, and A. R. Hamilton, *Phys. Rev. Lett.* **110**, 146803 (2013).

⁸ I. Amelio, N. D. Drummond, E. Demler, R. Schmidt, and A. Imamoglu, *Phys. Rev. B* **107**, 155303 (2023).

⁹ A. A. High, J. R. Leonard, M. Remeika, L. V. Butov, M. Hanson, and A. C. Gossard, *Nano Lett.* **12**, 2605 (2012).

¹⁰ L. V. Butov, A. C. Gossard, and D. Chemla, *Nature* **418**, 751 (2002).

¹¹ H. Cercellier, C. Monney, F. Clerc, C. Battaglia, L. Despont, M. G. Garnier, H. Beck, P. Aebi, L. Patthey, H. Berger, and L. Forró, *Phys. Rev. Lett.* **99**, 146403 (2007).

¹² A. Kogar, M. S. Rak, S. Vig, A. A. Husain, F. Flicker, Y. I. Joe, L. Venema, G. J. MacDougall, T. C. Chiang, E. Fradkin, J. van Wezel, and P. Abbamonte, *Science* **358**, 1314 (2017), <https://www.science.org/doi/pdf/10.1126/science.aam6432>.

¹³ J. F. Afonso and J. Kuneš, *Phys. Rev. B* **95**, 115131 (2017).

¹⁴ T. Moyoshi, K. Kamazawa, M. Matsuda, and M. Sato, *Phys. Rev. B* **98**, 205105 (2018).

¹⁵ J. Kuneš and P. Augustinský, *Phys. Rev. B* **90**, 235112 (2014).

¹⁶ L. Windgätter, M. Rösner, G. Mazza, H. Hübener, A. Georges, A. J. Millis, S. Latini, and A. Rubio, *npj Computational Materials* **7**, 210 (2021).

¹⁷ Y. Jia, P. Wang, C.-L. Chiu, Z. Song, G. Yu, B. Jäck, S. Lei, S. Klemenz, F. A. Cevallos, M. Onyszczak, N. Fishchenko, X. Liu, G. Farahi, F. Xie, Y. Xu, K. Watanabe, T. Taniguchi, B. A. Bernevig, R. J. Cava, L. M. Schoop, A. Yazdani, and S. Wu, *Nature Physics* **18**, 87 (2022).

¹⁸ B. Sun, W. Zhao, T. Palomaki, Z. Fei, E. Runburg, P. Malinowski, X. Huang, J. Cenker, Y.-T. Cui, J.-H. Chu, X. Xu, S. S. Ataei, D. Varsano, M. Palummo, E. Molinari, M. Rontani, and D. H. Cobden, *Nature Physics* **18**, 94 (2022).

¹⁹ S. De Palo, F. Rapisarda, and G. Senatore, *Phys. Rev. Lett.* **88** (2002), 10.1103/PhysRevLett.88.206401.

²⁰ P. López Ríos, A. Perali, R. J. Needs, and D. Neilson, *Phys. Rev. Lett.* **120**, 177701 (2018).

²¹ S. De Palo, F. Tramonto, S. Moroni, and G. Senatore, *Phys. Rev. B* **107**, L041409 (2023).

²² L. Rademaker, S. Johnston, J. Zaanen, and J. van den Brink, *Phys. Rev. B* **88** (2013), 10.1103/PhysRevB.88.235115.

²³ X. Huang, M. Claassen, E. Huang, B. Moritz, and T. Devereaux, *Phys. Rev. Lett.* **124** (2020), 10.1103/PhysRevLett.124.077601.

²⁴ X. Huang, B. Moritz, M. Claassen, and T. Devereaux, *Phys. Rev. B* **105** (2022), 10.1103/PhysRevB.105.165124.

²⁵ T. I. Vanhala, J. E. Baarsma, M. O. J. Heikkinen, M. Troyer, A. Harju, and P. Törmä, *Phys. Rev. B* **91**

- (2015), 10.1103/PhysRevB.91.144510.
- ²⁶ T. Kaneko, K. Seki, and Y. Ohta, Phys. Rev. B **85** (2012), 10.1103/PhysRevB.85.165135.
- ²⁷ J. Kuneš, Phys. Rev. B **89** (2014), 10.1103/PhysRevB.89.115134.
- ²⁸ J. Kuneš, Phys. Rev. B **90** (2014), 10.1103/PhysRevB.90.235140.
- ²⁹ J. Kuneš, J. Phys.: Condens. Matter **27** (2015), 10.1088/0953-8984/27/33/333201.
- ³⁰ A. Niyazi, D. Geffroy, and J. Kuneš, Phys. Rev. B **102**, 085159 (2020).
- ³¹ A. Amaricci, G. Mazza, M. Capone, and M. Fabrizio, Phys. Rev. B **107**, 115117 (2023).
- ³² A. Georges, G. Kotliar, W. Krauth, and M. Rozenberg, Rev. Mod. Phys. **63** (1996), 10.1103/RevModPhys.68.13.
- ³³ M. Caffarel and W. Krauth, Phys. Rev. Lett. **72**, 1545 (1994).
- ³⁴ M. Capone, L. de' Medici, and A. Georges, Phys. Rev. B **76**, 245116 (2007).
- ³⁵ A. Amaricci, L. Crippa, A. Scazzola, F. Petocchi, G. Mazza, L. de Medici, and M. Capone, Computer Physics Communications **273**, 108261 (2022).
- ³⁶ A. Koga, Y. Imai, and N. Kawakami, Phys. Rev. B **66** (2002), 10.1103/PhysRevB.66.165107.
- ³⁷ A. Isidori, M. Berović, L. Fanfarillo, L. de' Medici, M. Fabrizio, and M. Capone, Phys. Rev. Lett. **122**, 186401 (2019).
- ³⁸ A. Richaud, M. Ferraretto, and M. Capone, Phys. Rev. B **103**, 205132 (2021).
- ³⁹ A. Scazzola, A. Amaricci, and M. Capone, Phys. Rev. B **107**, 085131 (2023).
- ⁴⁰ D. J. Scalapino, S. R. White, and S. Zhang, Phys. Rev. Lett. **68** (1992), 10.1103/PhysRevLett.68.2830.
- ⁴¹ A. Toschi, M. Capone, and C. Castellani, Phys. Rev. B **72** (2005), 10.1103/PhysRevB.72.235118.
- ⁴² K. Seki, R. Eder, and Y. Ohta, Phys. Rev. B **84** (2011), 10.1103/PhysRevB.84.245106.

- ⁴³ T. Kaneko and Y. Ohta, Phys. Rev. B **90** (2014), 10.1103/PhysRevB.90.245144.
- ⁴⁴ G. Sangiovanni, A. Toschi, E. Koch, K. Held, M. Capone, C. Castellani, O. Gunnarsson, S.-K. Mo, J. W. Allen, H.-D. Kim, A. Sekiyama, A. Yamasaki, S. Suga, and P. Metcalf, Phys. Rev. B **73**, 205121 (2006).
- ⁴⁵ C. Taranto, G. Sangiovanni, K. Held, M. Capone, A. Georges, and A. Toschi, Phys. Rev. B **85**, 085124 (2012).
- ⁴⁶ G. Sangiovanni, M. Capone, C. Castellani, and M. Grilli, Phys. Rev. Lett. **94**, 026401 (2005).
- ⁴⁷ G. Sangiovanni, M. Capone, and C. Castellani, Phys. Rev. B **73**, 165123 (2006).
- ⁴⁸ P. Farkasovsky, Cond. Mat. Phys. **23** (2020), 10.5488/CMP.23.43709.
- ⁴⁹ P. Farkasovsky, Phys. Rev. B **65** (2002), 10.1103/PhysRevB.65.081102.

Appendix A: Superfluid Stiffness

In this appendix we provide some details of the calculation of the superfluid stiffness for the attractive model obtained through the canonical transformation (5). From the definition⁴⁰:

$$\frac{D_S}{\pi e^2} = \langle -E_{kin} \rangle - \chi_{jj}(\mathbf{q} \rightarrow 0, \omega = 0) \quad (\text{A1})$$

We need to compute the kinetic energy and the current-current response function. We make use of the previously defined spinorial representation to define the Green's function as:

$$\hat{G}_\sigma(\mathbf{k}, \tau) = \langle T \left(\begin{matrix} c_{kA\sigma}(\tau) \\ c_{kB\sigma}(\tau) \end{matrix} \right) \otimes (c_{kA\sigma}^\dagger(0) \ c_{kB\sigma}^\dagger(0)) \rangle = \begin{pmatrix} G_{AA}(\mathbf{k}, \tau) & G_{AB}(\mathbf{k}, \tau) \\ G_{BA}(\mathbf{k}, \tau) & G_{BB}(\mathbf{k}, \tau) \end{pmatrix} \quad (\text{A2})$$

From now on we consider it diagonal in the spin therefore we can avoid to write explicitly the spin index σ . In single-site DMFT, where the self-energy is local and site independent, the Dyson equation for the interacting Green's functions reads:

$$\hat{G}_0(\mathbf{k}, i\omega_n)^{-1} = \hat{G}(\mathbf{k}, i\omega_n)^{-1} + \hat{\Sigma}(i\omega_n) \quad (\text{A3})$$

where the hat indicates that all of these are matrices as in the previous equation A2. This means that the diagonal and off diagonal component are:

$$G_{AA}(\varepsilon, i\omega) = \frac{i\omega - \alpha\varepsilon - \Sigma_{BB}(i\omega)}{(i\omega - \varepsilon - \Sigma_{AA}(i\omega))(i\omega - \alpha\varepsilon - \Sigma_{BB}(i\omega)) - |\Sigma_{AB}(i\omega)|^2} \quad (\text{A4})$$

$$G_{BB}(\varepsilon, i\omega) = \frac{i\omega - \varepsilon - \Sigma_{AA}(i\omega)}{(i\omega - \varepsilon - \Sigma_{AA}(i\omega))(i\omega - \alpha\varepsilon - \Sigma_{BB}(i\omega)) - |\Sigma_{AB}(i\omega)|^2} \quad (\text{A5})$$

$$G_{AB}(\varepsilon, i\omega) = \frac{\Sigma_{AB}(i\omega)}{(i\omega - \varepsilon - \Sigma_{AA}(i\omega))(i\omega - \alpha\varepsilon - \Sigma_{BB}(i\omega)) - |\Sigma_{AB}(i\omega)|^2} = G_{BA}^*(\varepsilon, i\omega) \quad (\text{A6})$$

where $\alpha = t_B/t_A$ therefore $\epsilon^{(A)} = \epsilon$ and $\epsilon^{(B)} = \alpha\epsilon$.

In this derivation we will set the energy splitting to zero ($M = 0$) for simplicity but the results remain valid for any value of M . In DMFT the kinetic energy for orbital m can be easily computed since the Green's function is known:

$$E_{kin}^{(m)} = \sum_{\mathbf{k}\sigma} \epsilon_{\mathbf{k}}^{(m)} \langle c_{\mathbf{k}\sigma m}^\dagger c_{\mathbf{k}\sigma m} \rangle \quad (\text{A7})$$

$$\begin{aligned} &= \lim_{\eta \rightarrow 0^+} \beta^{-1} \sum_{i\omega_n} \sum_{\mathbf{k}\sigma} \epsilon_{\mathbf{k}}^{(m)} G_{mm}(\mathbf{k}, i\omega_n) e^{i\omega_n \eta} \\ &= \lim_{\eta \rightarrow 0^+} \beta^{-1} \sum_{i\omega_n, \sigma} \int d\epsilon D(\epsilon) \epsilon^{(m)} G_{mm}(\epsilon, i\omega_n) e^{i\omega_n \eta} \quad (\text{A8}) \end{aligned}$$

computing it explicitly for the two orbitals and performing a partial integration using the relation $-\epsilon D(\epsilon) = \partial_\epsilon [D(\epsilon)V(\epsilon)]$ where $V(\epsilon) = \frac{4t^2 - \epsilon^2}{3} = (v_\epsilon^{(A)})^2$ is the square of the current vertex in orbital A , $\alpha^2 V(\epsilon) = (v_\epsilon^{(B)})^2$ is the square of the current vertex in orbital B and $D(\epsilon) = \frac{1}{2\pi t^2} \sqrt{(2t)^2 - \epsilon^2}$ is the density of states:

$$\begin{aligned} E_{kin,A} &= \beta^{-1} \sum_{i\omega_n, \sigma} \int d\epsilon V(\epsilon) D(\epsilon) G_{AA}^2(\epsilon, i\omega_n) \left[1 + \alpha \frac{|\Sigma_{AB}(i\omega_n)|^2}{(i\omega_n - \alpha\epsilon - \Sigma_{BB}(i\omega_n))^2} \right] \\ &= \beta^{-1} \sum_{i\omega_n, \sigma} \int d\epsilon V(\epsilon) D(\epsilon) \left[G_{AA}^2(\epsilon, i\omega_n) + \alpha |G_{AB}(\epsilon, i\omega_n)|^2 \right] \quad (\text{A9}) \end{aligned}$$

$$\begin{aligned} E_{kin,B} &= \beta^{-1} \sum_{i\omega_n, \sigma} \int d\epsilon V(\epsilon) D(\epsilon) G_{BB}^2(\epsilon, i\omega_n) \left[\alpha^2 + \alpha \frac{|\Sigma_{AB}(i\omega_n)|^2}{(i\omega_n - \epsilon - \Sigma_{AA}(i\omega_n))^2} \right] \\ &= \beta^{-1} \sum_{i\omega_n, \sigma} \int d\epsilon V(\epsilon) D(\epsilon) \left[\alpha^2 G_{BB}^2(\epsilon, i\omega_n) + \alpha |G_{AB}(\epsilon, i\omega_n)|^2 \right] \quad (\text{A10}) \end{aligned}$$

$$(\text{A11})$$

From which one can check that if there is no orbital off-diagonal self-energy and $\alpha = \pm 1$ the kinetic energy is the same in the two orbitals. The computation of the current-current response in DMFT in infinite dimensions is sim-

plified since all the vertex corrections are cancelled³² and only the elementary bubble contributions survive, therefore:

$$\chi_{jj}(\mathbf{q}, \tau) = - \langle j_{ex}(\mathbf{q}, \tau) j_{ex}(-\mathbf{q}, 0) \rangle, \quad j_{ex}(\mathbf{q}, \tau) = j_A(\mathbf{q}, \tau) - j_B(\mathbf{q}, \tau) \quad (\text{A12})$$

$$\chi_{jj}(\mathbf{q} \rightarrow 0, i\omega = 0) = [\chi_{jj}^{AA} - \chi_{jj}^{AB} - \chi_{jj}^{BA} + \chi_{jj}^{BB}](\mathbf{q} \rightarrow 0, i\omega = 0) \quad (\text{A13})$$

$$\chi_{jj}^{mm'}(\mathbf{q}, i\omega) = -\beta^{-1} \sum_{\mathbf{k}, i\nu, \sigma} v_{\mathbf{k}\sigma}^{(m)} v_{\mathbf{k}+\mathbf{q}\sigma}^{(m')} G_{mm'}(\mathbf{k}, i\nu) G_{m'm}(\mathbf{k} + \mathbf{q}, i\nu + i\omega), \quad m, m' = A, B \quad (\text{A14})$$

$$(\text{A15})$$

Where the current vertex for the two orbitals are related by $v^{(B)} = \alpha v^{(A)}$. Merging the DMFT results for the

kinetic energy and the current-current response function, the superfluid stiffness for the selected model is:

$$\frac{D_S}{e^2 \pi} = -\frac{4\alpha}{\beta} \sum_{i\omega_n, \sigma} \int d\epsilon V(\epsilon) D(\epsilon) |G_{AB}(\epsilon, i\omega_n)|^2 \quad (\text{A16})$$

This interesting result carries some important informa-

tion. Since the *Superfluid Stiffness* has to be a positive

quantity, the "naive" two-orbital Hubbard model with symmetric bands ($\alpha = 1$) would not allow any finite D_S , this is in agreement with some results showing that local excitonic correlations are dumped for $\alpha > 0$ ⁴⁸ in favor of a bipartite antiferro-EC state that correspond to a model with a shift of the B band of the vector \mathbf{Q} of bipartite lattices for which $\epsilon_{\mathbf{k}} = -\epsilon_{\mathbf{k}+\mathbf{Q}}$, e.g. for the square lattice in D -dimensions the vector is $\mathbf{Q} = (\pi, \pi, \dots, \pi)$. For $\alpha = 0$ (Falikov-Kimball Model with spin) it correctly predict no superfluid excitonic state since one of the species is not mobile and since in this limit no excitonic phase is expected⁴⁹. This special case prohibit excitonic ordering since in the limit $\alpha \rightarrow 0^+$ there must be an antiferro-EC state while in the limit $\alpha \rightarrow 0^-$ a ferro-EC state, thus $\alpha = 0$ is an unstable point between these two phases²⁹. Our choice of opposite bands $\alpha = -1$ is therefore optimal and in this situation the Superfluid Stiffness can be

rewritten as:

$$\frac{D_S}{e^2\pi} = \frac{4}{\beta} \sum_{\sigma, i\omega_n} \int d\epsilon V(\epsilon) D(\epsilon) |G_{AB}(\epsilon, i\omega_n)|^2 \quad (\text{A17})$$

This results tells us that opposite band dispersion is the optimal ground for the research of a Superfluid Exciton Condensate.

Appendix B: Calculation of the Coherence Length

For the Bethe lattice we have no access to the momenta but only energy, therefore we have to pass from $\nabla_{\mathbf{k}}$ to something we can treat. Starting from the numerator of the coherence length definition^{42,43}:

$$\sum_{\mathbf{k}} \left| \nabla_{\mathbf{k}} F(\mathbf{k}) \right|^2 = \sum_{\mathbf{k}} \left| (\nabla_{\mathbf{k}} \epsilon_{\mathbf{k}}) \frac{\partial F(\epsilon)}{\partial \epsilon} \Big|_{\epsilon=\epsilon_{\mathbf{k}}} \right|^2 = \sum_{\mathbf{k}} \left| (\nabla_{\mathbf{k}} \epsilon_{\mathbf{k}}) \left[\frac{1}{\beta} \sum_{i\omega_n} e^{i\omega_n 0^+} \frac{\partial}{\partial \epsilon} F(\epsilon, i\omega_n) \Big|_{\epsilon=\epsilon_{\mathbf{k}}} \right] \right|^2, \quad (\text{B1})$$

where $F(\epsilon, i\omega_n) = G_{AB}(\epsilon, i\omega_n)$ as previously defined (See Appendix A) and $\nabla_{\mathbf{k}} \epsilon_{\mathbf{k}} = v_{\mathbf{k}}$ is the group velocity of the non interacting particles (we take $\hbar = 1$). Now the de-

pendency on \mathbf{k} is present only through $\epsilon_{\mathbf{k}}$ via the relation $|v_{\mathbf{k}}| = \sqrt{\frac{4t^2 - \epsilon_{\mathbf{k}}^2}{3}} = v(\epsilon)$ therefore we can pass to the integral in energy and the result for the numerator is:

$$\sum_{\mathbf{k}} \left| \nabla_{\mathbf{k}} F(\mathbf{k}) \right|^2 = \int d\epsilon D(\epsilon) \left| \frac{1}{\beta} \sum_{i\omega_n} e^{i\omega_n 0^+} v(\epsilon) G_{AB}^2(\epsilon, i\omega_n) \frac{2\epsilon + \Sigma_{BB}(i\omega_n) - \Sigma_{AA}(i\omega_n)}{\Sigma_{AB}(i\omega_n)} \right|^2 \quad (\text{B2})$$

For the denominator no change is needed and the substi-

tution of $F(\mathbf{k})$ gives directly

$$\int d\epsilon D(\epsilon) \left| \frac{1}{\beta} \sum_{i\omega_n} e^{i\omega_n 0^+} G_{AB}(\epsilon, i\omega_n) \right|^2 \quad (\text{B3})$$